A 2-bit 3D-Printed Reflectarray Antenna Using Cylindrical Rotation-Based Phase Tunable Elements

Ao Hu, *Graduate Student Member, IEEE,* Keisuke Konno, *Member, IEEE,* and Qiang Chen, *Senior Member, IEEE*

***Abstract*—In this paper, a low-cost and mechanically robust approach for the design of mechanically phase-tunable reflectarray elements operating in the C-band is proposed. The proposed element composes of an open cylindrical shell made of a non-uniform dielectric material. A 2-bit phase tunability is achieved by implementing mechanical rotation of the open cylindrical shell. The proposed element is fabricated by 3D-printing technology, and infill rate of the open cylindrical shell is spatially non-uniform. As a result, effective relative permittivity of the fabricated open cylindrical shell becomes non-uniform. Phase tunability of the fabricated element is demonstrated numerically and experimentally. A reflectarray antenna composed of the proposed elements is designed and fabricated. It is clarified that the reflectarray antenna demonstrates beam scanning coverage up to 50° while its aperture efficiency is comparable to conventional reflectarray antennas.**

***Index Terms*—Reflectarrays, additive manufacturing, antennas, arrays.**

I. Introduction

A reflectarray (RA) antenna is a class of reflector antennas, which are composed of numerous reflecting elements and a primary source. The reflecting elements are typically designed so that the scattering wave from the reflecting elements is in-phase at a specific direction. The first RA antenna is composed of an array of variable-length waveguides [1]. Although the first RA antenna is bulky and heavy, owing to the advancement of wireless communication systems, various planar RAs have been extensively studied due to their low-profile and high gain features [2]–[4].

In previous studies, the passive RAs were developed for various applications. In particular, the passive RAs have been applied to eliminate blindness of the wireless communication systems. A RA composed of non-identical planar dipole elements with parasitic elements was developed to eliminate blindness in a CDMA (WCDMA) communication system [5]. Two RAs whose reflecting surface were perpendicular to each other was proposed to improve signal coverage in a cornered corridor [6]. A RA composed of groove shaped elements was developed so that it can guide the incident field to the end-fire direction of the RA surface [7]. Although the passive RAs have capability to eliminate the blindness, their performance is not tunable once they are fabricated.

Manuscript received 30 January 2024; revised 27 June 2024; accepted 22 August 2024. *(Corresponding author: Keisuke Konno.)*

A. Hu, K. Konno and Q. Chen are with the Department of Communications Engineering, Graduate School of Engineering, Tohoku University, Sendai 980-8579, Japan (e-mail: hu.ao.p7@dc.tohoku.ac.jp).

Color versions of one or more figures in this article are available at https://doi.org/xx.xxxx/TAP.xxxx.xxxxxxx

Digital Object Identifier xx.xxxx/TAP.xxxx.xxxxxxx

In order to overcome the lack of tunability of the passive RAs, reconfigurable (or active) RAs have been proposed. Electronically reconfigurable RA is well-known as one of the popular approaches for designing the reconfigurable RA. Traditionally, varactor diodes or pin diodes have been introduced to the electronically reconfigurable RAs so that their aperture phase distribution is tunable [8]–[11]. Recently, 1-bit time modulation has been introduced to a RA for reducing its sidelobe level [12]. Electronically reconfigurable RAs based on new technologies such as using microelectromechanical system (MEMS) switches [13] [14] and liquid crystal [15] [16] were proposed. Insertion loss, quantization loss, and resultant low aperture efficiency are typical disadvantages of the electronically reconfigurable RAs whereas high-speed reconfigurability and high system integration ability are their major advantages [17]. It has been demonstrated that the quantization loss can be enhanced by loading multiple number of the diodes with the RA elements [18], [19]. However, enhancement of the quantization loss can be hardly achievable without the expense of the cost and the complexity of bias circuits.

Mechanically reconfigurable RA using actuators or motors is another promising approach for designing the reconfigurable RA. Notable examples of mechanically reconfigurable RAs include variations in the height of patch elements [20] [21], bending a dipole strip element using electromagnet [22], rotation of specific parts of the reflecting elements [23], [24], and the controlled deformation of flexible element through squeezing [25]. While mechanically reconfigurable RAs offer continuous phase shift, high fabrication cost (e.g. multiple number of actuators/motors or precise mechanical control system) or complicated shape of the RA elements are major disadvantages. To reduce the fabrication cost of the mechanically reconfigurable RAs, various RAs with the small number of actuators have been developed. For instance, a deformable ground plane actuated by only four motors was introduced [26]. A beam scanning RA by rotating the whole RA, not each RA element by single motor was proposed [27]. A beam scanning RA by actuating cascading elements using Archimedean spiral cam with single motor was designed [28]. Although the advancements on reducing fabrication cost are found, the cost-effective fabrication technologies for complicated shape of the RA elements are expected to be developed.

Owing to the recent advancements on additive manufacturing technologies, the complicated shape RA elements can be fabricated at low cost as 3D-printed RAs have been widely developed. For example, 3D-printing technologies allows the fabrication of different thickness dielectric elements [29],

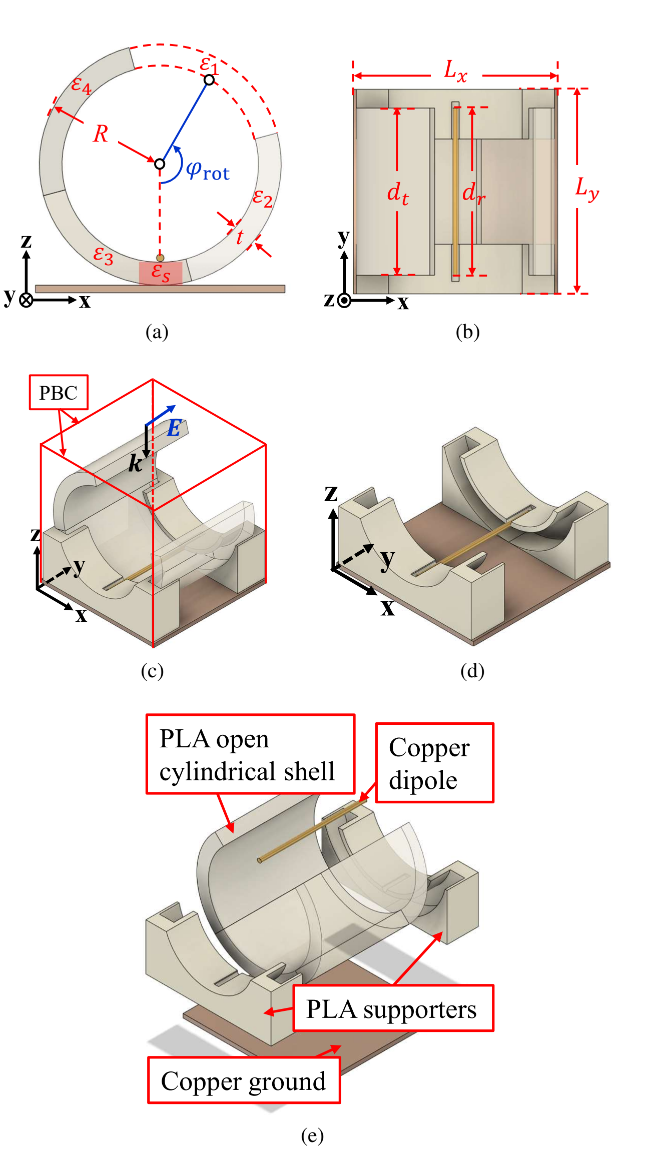

Fig. 1. The configuration of cylindrical RA element (a). Front view (Illustration of the PLA supporters are omitted here for visibility), (b). Top view, (c). Birds eye view, (d) Birds eye view with cylinder shell omitted and (e). Exploded view.

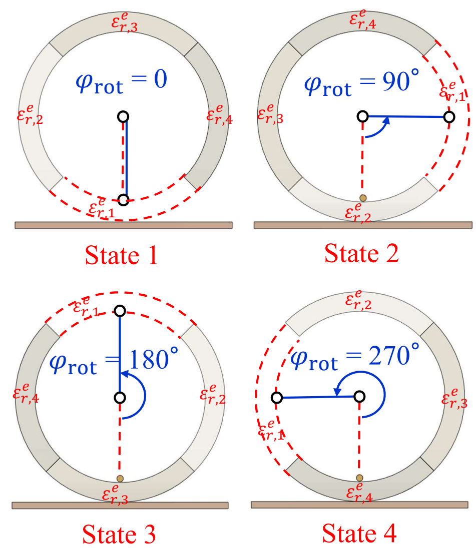

Fig. 2. 2-bit phase tunable mechanism of the proposed RA element under different rotation angle φ_{rot}. (Illustration of the PLA supporters are omitted here for visibility).

multi-layer structure [30], infill rate adjusted lattice element [31], and printed nonradiative dielectric waveguide structure [32]. Efforts on elements with wide band response such as LPDA have been made by 3D-printing technique to overcome the narrow band property of conventional planar reflecting elements [33] [34]. Moreover, the adoption of 3D-printing techniques substantially reduces the fabrication costs associated with complex structures, providing a freedom in the design of reflecting elements. The 3D-printing technologies are powerful technologies for efficient fabrication of the RA elements with complicated geometry. However, most of the previous 3D-printed RAs are passive ones, not reconfigurable ones except for deployable RAs proposed in [25]. Although the deployable RA enables to transform their shape from folded one to deployed one, beam scanning capability is unavailable because the RA element lack of the ability to individually tunning the phase. Therefore, low-cost mechanically reconfigurable 3D-printed RAs are still expected to be developed.

In this paper, we propose a 2-bit 3D-printed RA element. The proposed element is composed of an open cylindrical shell of a dielectric material whose relative permittivity is non-uniform. Phase tunability of the proposed element is realized by rotating the open cylindrical shell mechanically. The open cylindrical shell is fabricated using the low-cost 3D-printed technology and non-uniform effective relative permittivity is achieved by printing non-uniform infill rate of material. Robust 2-bit phase tunability with respect to error of a rotation angle, which is an advantage of the proposed RA element, is demonstrated. The robust phase tunability contributes to reduce cost of mechanical control system because precise control of the rotation angle is unnecessary. Of course, the low-cost 3D-printed technology also contributes to reduce the fabrication cost.

The following sections are organized as below: In section II, a cylindrical RA element is proposed and designed. Next, prototypes of the cylindrical RA elements are fabricated, and their 2-bit phase shift performance is clarified numerically and experimentally. In Section III, a 10 $\times$10 RA antenna with conceptual automation of rotation system is proposed, a prototype using the proposed elements is fabricated and the primary source position is optimized. In Section IV, beam steering performance of the fabricated prototype is measured in a radio anechoic chamber and the measured results are discussed. Finally, Section V concludes this work.

II. Design and Validation of Cylindrical Element

A. Design and Working Principle of the RA Element

The configuration of the proposed cylindrical RA element is illustrated in Fig. 1. The proposed element is composed of a dipole element enclosed by an open cylindrical shell of dielectric material, which is on a ground plane. Height,

This article has been accepted for publication in IEEE Transactions on Antennas and Propagation. This is the author's version which has not been fully edited and content may change prior to final publication. Citation information: DOI 10.1109/TAP.2024.3451133

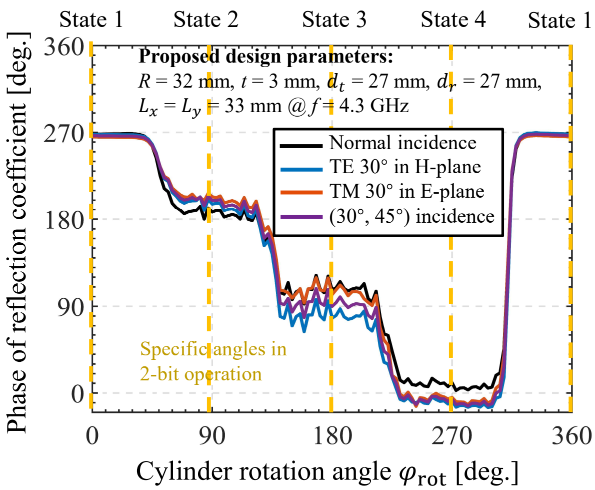

(a)

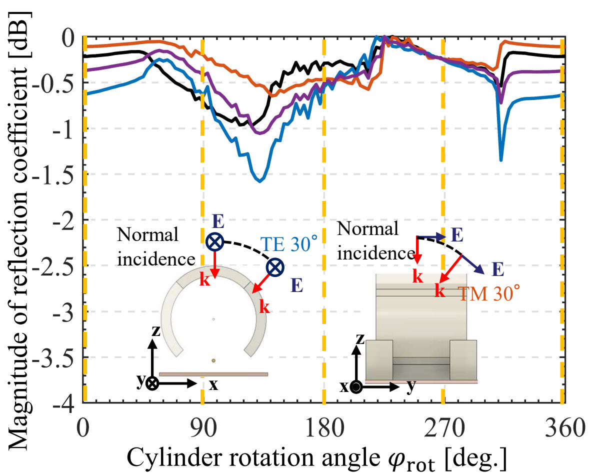

(b)

Fig. 3. Tunability of reflection coefficient with respect to open cylindrical shell rotation angle φ_{rot}. Specific angles of rotation corresponding to 2-bit operation are indicated by vertical yellow dashed lines.

diameter, and thickness of the open cylindrical shell are denoted as d_t, R, and t, respectively. Internally, the open cylindrical shell is made of four different dielectric media including vacuum (i.e. open part), and PLA walls with three different infill rates. Effective relative permittivity of the four different medium shown in Fig.1 are denoted as $\epsilon^e_{r,n}$, where n = 1,2,3,4.

A copper dipole with a length d_r fixed on PLA supporters is inside the open cylindrical shell, which is depicted in Fig. 1(d) in detail. In Fig. 1(d), the open cylindrical shell is omitted for enhancing visibility. The PLA supporters are slotted to support the dipole. The open cylindrical shell is freely rotatable around the dipole element because mechanical connection between them is absent. Rotation angle of the open cylindrical shell is denoted by φ_{rot}. Observing toward y-direction, the counter clock-wise rotation angle φ_{rot} is defined from the $-z$-direction to the blue line pointing to the center of vacuum part, as depicted in Fig. 1(a). Owing to the PLA supporters, position of the copper dipole is kept during rotation of the open cylindrical shell. Size of the copper ground in x-directon is L_x and that

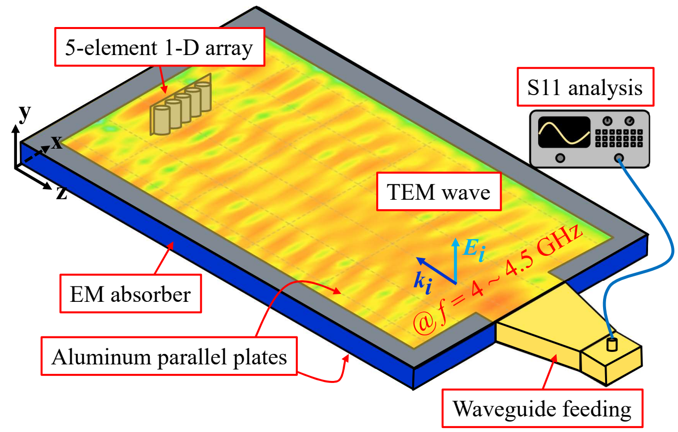

Fig. 4. The PPW measurement setup for validating the reflection coefficient of a one-dimensinal five-elements array.

in y-direction is L_y.

The phase tuning mechanism of this cylindrical element is based on the substrate-tunable resonator approach [35]. This mechanism involves dynamically tuning the relative permittivity of the substrate between the dipole and ground. Here, the dynamic tunability is achieved by rotating the open cylindrical shell made of four different dielectric medium including vacuum (i.e. open part), and PLA walls with three different effective relative permittivity. In this paper, design and fabrication of RA using the proposed RA element are performed in C-band because of limited accuracy (or tolerance) of a 3D-printer for fabrication. 2-bit phase tunable mechanism of the proposed RA element is shown in Fig. 2. As the open cylindrical shell is rotated, it is expected that the phase of reflection coefficient of the proposed RA element changes because the effective relative permittivity of the substrate between the dipole element and the ground changes. Therefore, four sections of cylinder shell are expected to achieve 2-bit of phase shift.

Practically, it is well-known that PLA walls with non-uniform effective relative permittivity can be fabricated by the 3D-printing technology when infill rate inside the walls is controlled [36]. Here, the effective relative permittivity of the four different media inside the open cylindrical shell can be expressed as follows:

$$\epsilon^e_{r,n} = \mathrm{Re}[\epsilon_{\mathrm{r}}]\rho_{\mathrm{n}} + 1 - \rho_{\mathrm{n}}, \tag{1}$$

where ρ_n is the infill rate at medium n and the ϵ_r denotes the complex relative permittivity of the PLA (= 2.7 + j0.01 @f = 4.3 GHz). According to the expression, the effective relative permittivity of the media inside the shell are designed as follows: $\epsilon^e_{r,1} = 1$ (ρ_1 = 0%), $\epsilon^e_{r,2} = 1.48$ (ρ_2 = 28.2%), $\epsilon^e_{r,3} = 1.77$ (ρ_3 = 45.3%) and $\epsilon^e_{r,4} = 2.7$ (ρ_4 = 100%).

B. Scattering Performance of Proposed RA Element

The scattering performance of the proposed RA element was simulated under the periodic boundary condition (PBC) by the commercial simulator software FEKO based on the Method of Moments (MoM). Here, operating frequency of

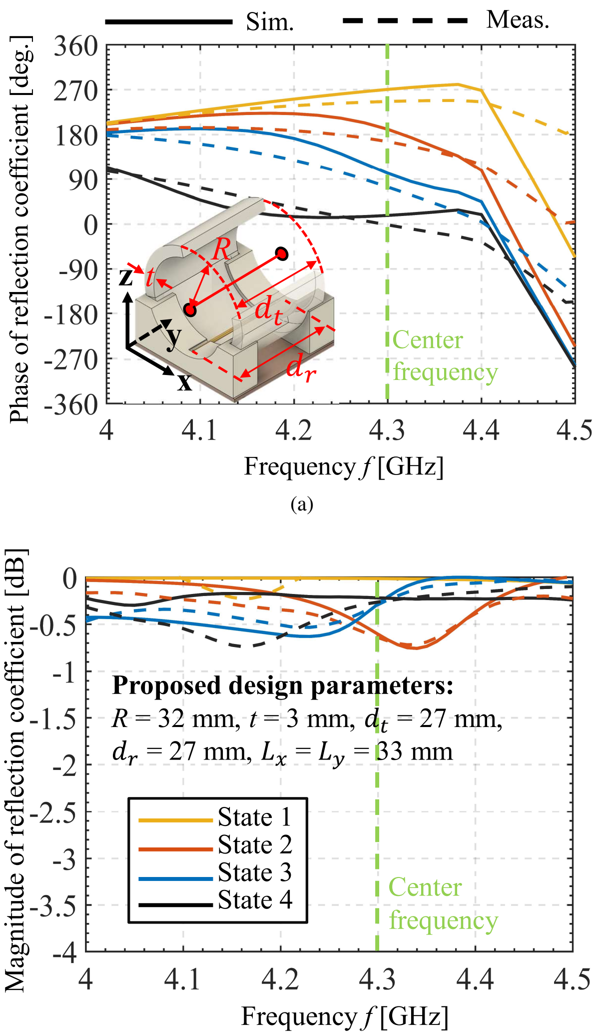

Fig. 5. Frequency response of reflection coefficient of the proposed RA element.

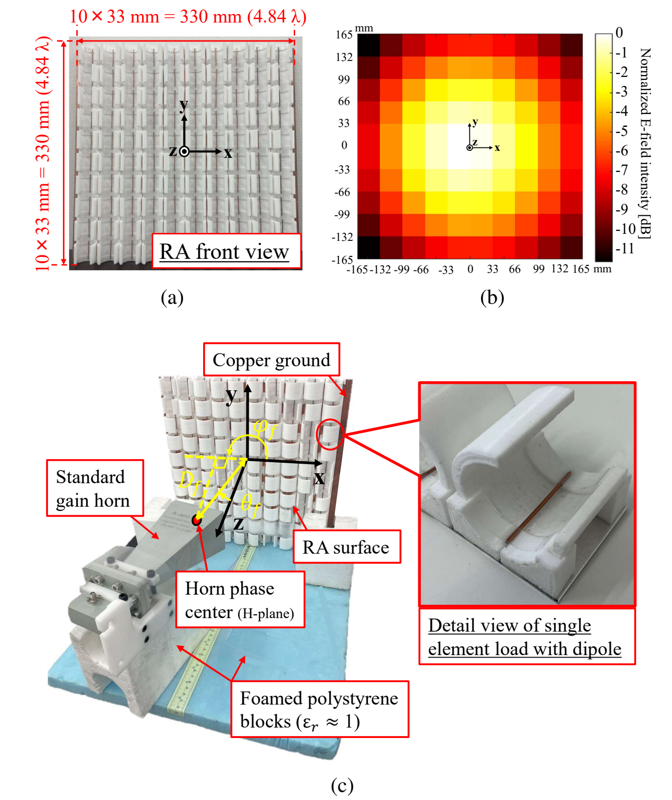

Fig. 6. Fabricated 10×10 (= 100) elements RA antenna prototype (a). front view, (b) Illumination level over the RA surface and (c) RA illuminated by a horn antenna. Here, λ is wavelength at f = 4.3 GHz.

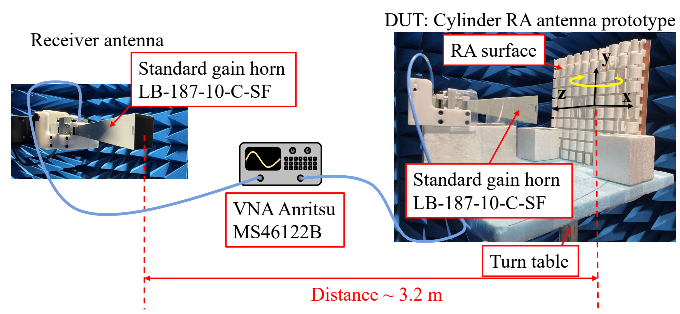

Fig. 7. A side-viewed demonstration of the beam steering performance measurement setup for measuring the proposed RA antenna system.

the RA element is 4.3 GHz and its array spacing in x- and y-directions are L_x = L_y = 33 mm (0.473λ). Amplitude variation and phase shift of the reflection coefficient along with the rotation angle φ_{rot} are demonstrated in Fig. 3. As the open cylindrical shell rotates, an obvious 2-bit staircase like phase shift was observed for reflection coefficients corresponding to all of the incident angles. According to phase shift of the reflection coefficient corresponding to incident angle (θ, φ) = (30°, 45°), whereas polarization is TE that E-field only has 45° φ-component, beam scanning capability outside E- and H- planes is expected to the RA using the proposed element. Small ripples appear on the phase shift because the phase of reflection waves from fixed parts (i.e. dipole, supporters, and ground) and a rotated part (i.e. open cylindrical shell) of the RA element changes respectively due to mutual coupling as the open cylindrical shell rotates. The worst ripple on the phase shift is found around 180° and its level is approximately $\pm$30°. The level of the ripples is within $\pm$45° and can be tolerated for the 2-bit operation. The staircase like phase shift and the small level of the ripples within $\pm$45° contribute to the robust 2-bit phase tunability. As a result, requirements on accuracy of positioning of the open cylindrical shell are alleviated and high-speed rotation is achievable because rotation speed and accuracy is tradeoff. On the other hand, the magnitude drop of the reflection coefficient was at most 1.6 dB when the open cylindrical shell fully rotates. As for fixed angle in 2-bit operation, the magnitude drop was at most 0.8 dB. The observed magnitude drop stems from the loss of the PLA. According to the numerical results shown here, it is found that the proposed RA element demonstrates 2-bit phase shift with small loss less than 0.8 dB.

Next, frequency response of the reflection coefficient of the proposed RA element is measured. The measurement system using a parallel plate waveguide (PPW) is shown in Fig. 4. In the same manner as a rectangular waveguide, the PPW

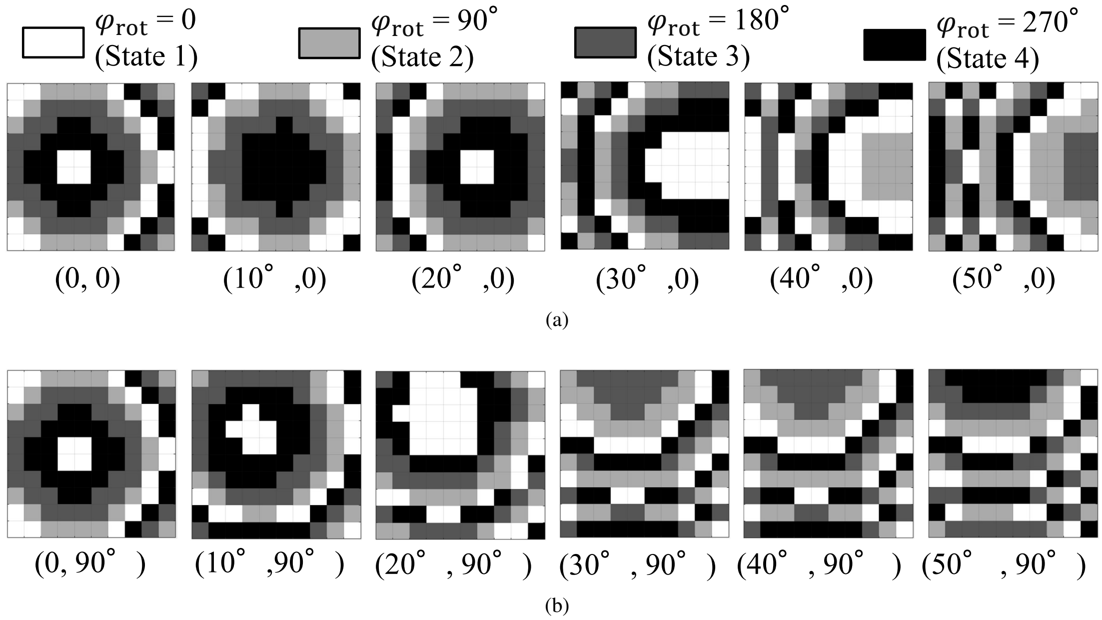

Fig. 8. The assigned rotation angle φ_{rot} to each element of the proposed RA antenna system for main beam direction (θ_s, φ_s) steering in (a). xoz-plane (φ_s = 0), and (b). yoz-plane (φ_s = 90°).

has been used for measurement of reflection/absorption of a device under test (DUT) inside the PPW [37]–[39]. It is well-known that TEM wave propagates inside the PPW if parallel plates are infinitely large. However, in practice, the size of the parallel plates is finite and so-called edge effect appears around the edge of the PPW. As a result, planar wave front can be kept in a limited area inside the PPW whereas it is not kept around its edge because of the effect of reflection wave from the edge. Numerical simulation was performed in advance of measurement, and it is found that planar wave front can be kept in a central area inside the PPW whose size is approximately comparable to five elements array of the proposed RA element along with x-direction as shown in Fig. 4. The PPW is composed of two aluminum plates, and the edges of the PPW were terminated by radio wave absorbers so that the effects of reflection waves from the edges are negligible. A 5-element 1-dimensional RA composed of the proposed RA elements was fabricated using a Flash Forge Guider 2s industrial level 3D printer. During the measurement, the fabricated RA was inside the PPW and rotation angle of the all RA elements were the same (i.e. φ_{rot} = 0, 90°, 180°, and 270°). Reflection coefficient of the fabricated RA was measured and normalized by that of the metal plate with the same size ($5L_x \times L_y$ = 165×33 mm^2).

The measured frequency response of the reflection coefficients is shown in Fig. II-A. In order to validate the measured results, simulated results using MoM under the PBC are also shown in Fig. II-A. According to the results, it is found that the 2-bit phase tunability is available over the 4.3 GHz band at the expense of small loss less than 0.8 dB. The simulated and measured results shown here demonstrate significant potential of the proposed RA elements.

III. Design and Fabrication of RA Antenna

A. Fabrication and Assemble of Planar RA

Fig. 6(a) shows a fabricated prototype of a planar RA with 10×10 elements. The open cylindrical shells and their supporters were fabricated using the Flash Forge Guider 2s 3D printer. The fabricated RA is backed by a copper ground plane and the dipole elements are made of copper wire with a diameter of 1 mm. A detailed view of single element is shown on the right-hand side in Fig. 6(c), where the dipole was inserted and taped in the slot of the PLA supporter so that their position is stationary as the open cylindrical shell rotates.

This paper focuses on demonstrating radiation performance of the RA antenna with the proposed elements and development of the automatic rotation system for the open cylindrical shell is beyond the scope of this paper. Therefore, all of the RA elements were rotated manually during the measurement. In practice, the automatic rotation system using actuators or motors are expected to be developed but its development is future work.

B. Illumination Source and RA System Optimization

The final configuration of the RA antenna system is presented in Fig. 6(c), where foamed polystyrene blocks ($\epsilon_r \approx 1$) are employed to integrate the proposed RA and the primary source. The primary source is a standard gain horn antenna (A-INFO LB-187-10-C-SF) [40]. The yellow coordinate system (D_f, θ_f, φ_f) denotes the relative position of the primary source to the proposed RA. The parameter D_f represents the spacing between the standard gain horn H-plane phase center and the geometrical center of the proposed RA. θ_f and φ_f are offset angles of the primary source from z-axis and x-axis, respectively.

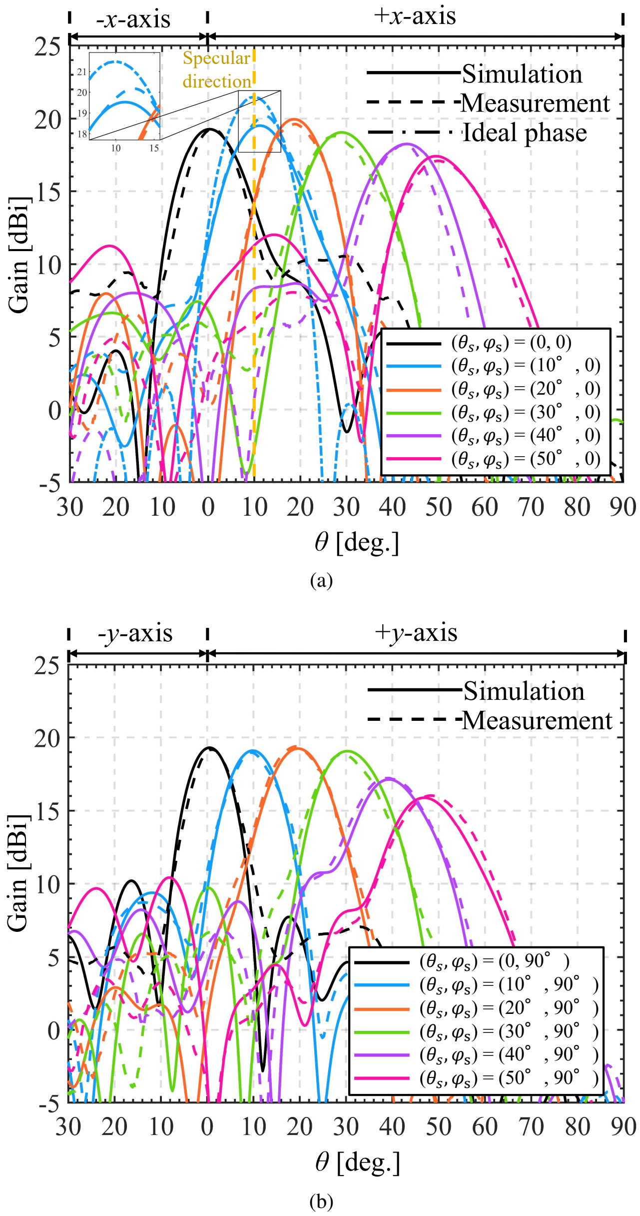

Fig. 9. Gain patterns of the proposed RA antenna at f = 4.3 GHz for the main beam directed in (a). xoz-plane (φ_s = 0), and (b). yoz-plane (φ_s = 90°). The solid lines represent the simulation results and the dashed lines represent the measurement results.

Relative position of the primary source to the proposed RA is optimized in advance of measurement so that its aperture efficiency becomes as high as possible at f = 4.3 GHz. At first, the offset angles are chosen as (θ_f, φ_f) = (10°, 180°) in order to avoid feed blockage in broadside direction. Next, D_f is optimized in the same manner as our previous publication [22]. As a result of optimization, D_f = 210 mm is chosen and 72 % aperture efficiency is expected ideally (so-called F/D ratio, i.e. ratio between D_f and dimension of RA, is approximately 0.64). Fig. 6(b) shows illumination level over the RA surface. Taper levels are -6 dB at the edge and -12 dB at the corner, respectively. The detailed optimization process here is omitted and interested readers can refer to [22] and [3].

The proposed RA antenna focusing its main beam to (θ, φ) = (θ_s, φ_s) is designed using following formula [3]:

$$\Psi_i = k\left(R_i - \boldsymbol{r}_i \cdot \hat{\boldsymbol{r}}_s\right) + \Psi_0, \tag{2}$$

where Ψ_i is the ideal phase of reflection coefficient of the i^{th} element, k is the free space wavenumber, R_i is the spacing from the primary source phase center to the i^{th} element, $\boldsymbol{r}_i$ is the position vector of the i^{th} element element, and $\hat{\boldsymbol{r}}_s$ is unit vector directed toward main beam direction (θ_s, φ_s). The term Ψ_0 represents the bias phase, an additional degree of freedom obtained to maximize the gain of the proposed RA antenna [41].

According to the relationship between phase of reflection coefficient of the proposed RA element and φ_{rot} shown in Fig. II-A, the rotation angle of the i^{th} element φ^i_{rot} is determined in 2-bit manner as follows:

$$\varphi^i_{\mathrm{rot}} = \begin{cases} 0 & , \Psi_i \in [225°, 315°] \\ 90° & , \Psi_i \in [135°, 225°] \\ 180° & , \Psi_i \in [45°, 135°] \\ 270° & , \Psi_i \in [0°, 45°] \cup [315°, 360°]\,. \end{cases} \tag{3}$$

The radiation performance of the fabricated RA antenna was measured in a radio anechoic chamber as shown in Fig. 7. During the measurement, a time-domain gating function was applied to filter the direct wave from the primary source to the receiving antenna.

The gain patterns of the proposed RA antenna are demonstrated in Fig. 9. States of RA elements corresponding to main beam directions are shown in Fig. 8. In order to validate the measurement results, simulated results obtained using MoM are also shown in Fig. 9. Agreement between the measured gains and the simulated ones is found. For example, in the specular reflection scenario, where the main beam is steered to (θ_s, φ_s) = (10°, 0), the gain reaches 20.2 dBi at maximum, with the first side-lobe level at -13.0 dB. On the other hand, as the main beam direction is steered to θ_s = 50°, the gain pattern distorts, and a grating lobe appears at around (θ, φ) = (20°, 180°). The distortion comes from error in phase compensation at large steering angle due to the effect of mutual coupling. Precise phase compensation over wide steering angle is a big challenge and future work. The aperture efficiency of the proposed RA antenna system in the specular reflection scenario is approximately 37.0%. The loss budget of the gain performance is presented in Table. I, where the losses in illumination, spillover, and phase quantization are elaborated. The loss of the illumination and the spillover have been already included in the estimated efficiency in Section III-B. The phase

TABLE I
GAIN LOSS BUDGET OF THE PROPOSED RA ANTENNA WHEN BEAM STEERING TO (θ_s, φ_s) = (10°, 0).

Parameter	Value
Maximum directivity ($4\pi A/\lambda^2$)	24.5 dBi
Illumination	0.7 dB
Spillover	0.8 dB
Phase quantization	1.3 dB
Feed blockage, phase error, material loss, others	1.5 dB
Total loss	4.3 dB
Gain (Aperture efficiency)	20.2 dBi (37%)

TABLE II
COMPARISON AMONG THE REPORTED RA AND RA ANTENNAS.

Related reference	Frequency [GHz]	Phase tuning mechanism	Manufacture method	Phase resolution	Element loss [dB]	Cross polar component [dB]	Profile [λ]	Aperture efficiency [%]	Scanning range [deg.]
[8]	5.8	Varactor	PCB process	Continuous	3.5	N.G.	0.04	N.A.	±40
[10]	5	Diode	PCB process	1-bit	1	-25	0.045	15.3	±50
[20]	4.8	Height tunning	Metal process	Continuous	0.18	-27	N.G.	48.6	±60
[24]	8.3	Element rotation	Metal process	3-bit	0.2	-23	N.G.	51.8	±60
[29]	100	**Tunable dielectric**	**3D-printing**	N.A.	0.7	N.G.	0.83	∼15.5	N.A.
[30]	66	**Tunable dielectric**	**3D-printing**	N.A.	0.5	-30	1.65	∼43.9	N.A.
This work	4.3	**Tunable dielectric**	**3D-printing**	2-bit	0.8	-25	0.5	37.0	**±50**

N.G.= not given, N.A.= not applicable.

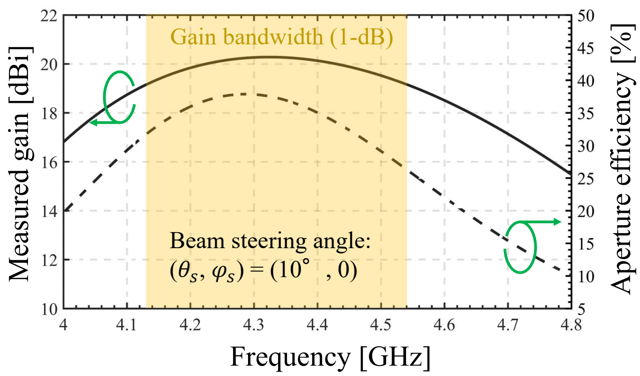

(a)

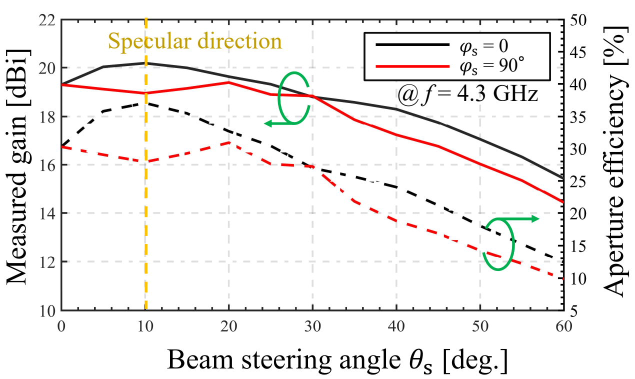

(b)

Fig. 10. Measured gain performance of the proposed RA antenna system (a). versus the frequency f, (b). versus the beam steering angle θ_s in both xoz- and yoz-planes.

quantization loss was obtained by subtracting the simulated gain of the proposed RA with ideally compensated phase from the 4-state compensated ones. The simulated gain pattern on the specular direction with ideally compensated phase is shown in Fig. 9(a). According to Fig. 9(a), it is found that quantization loss of the proposed RA element is approximately 1.3 dB. The remaining loss corresponds to feed blockage, phase error, material loss, others.

IV. Measurement of Radiation Performance

The frequency responses of the measured gain and aperture efficiency of the proposed RA antenna, corresponding to specular reflection, are presented in Fig. 10(a). Fractional bandwidth corresponding to the 1 dB gain drop of the RA antenna system is approximately 412 MHz, corresponding to a fractional bandwidth of about 9.2%. The 1 dB gain drop bandwidth of the proposed RA antenna is wider than that of conventional microstrip RAs (Approximately, 3∼5% in [42], [43]) but is narrower than that of 3D printed ones (>10% in [33], [34]). Such moderate bandwidth of the proposed RA antenna can be explained by following two reasons. At first, the proposed RA element has a relatively large profile rather than conventional microstrip one. The thicker profile contributes to enhance the bandwidth of the proposed RA antenna. Secondly, the proposed RA element quantize the phase in 2-bit, not continuous one. The phase quantization of the proposed RA element results in the limitation of the bandwidth. As a result, the proposed RA antenna demonstrates relatively moderate bandwidth.

The beam scan loss of the proposed RA antenna is depicted in Fig. 10(b). When steering the beam in the xoz-plane (φ_s = 0), the measured gain decreases as the beam steering angle θ_s shifts from the specular direction. For scenarios where (θ_s, φ_s) = (60°, 0) and (60°, 90°), the corresponding gains are approximately 15.4 dBi and 14.4 dBi, resulting in scan losses of 4.8 dB and 5.8 dB, respectively. According to the results, it can be said that scan loss increases as the main beam direction approaches to 90°. The increase of scan loss stems from reduction of RA aperture area, the presence of grating lobes, and phase compensation error.

Finally, a comparison of the proposed RA antenna with some representative references works is summarized in Table. II. From the comparison, it is shown that the proposed RA demonstrate beam steering ability while the aperture efficiency is comparable to those of related references.

V. Conclusion

A low-cost mechanically phase tunable RA element was proposed. The proposed RA element is composed of an open cylindrical shell made of dielectric material with a non-uniform relative permittivity, phase tunability of the proposed RA element is achieved by rotating the open cylindrical shell. The open cylindrical shell with the non-uniform relative permittivity was fabricated using 3D-printing technology by controlling infill rate. Numerical simulation and measurement were performed, and 2-bit phase shift performance of the proposed RA element was demonstrated. Finally, the RA antenna composed of the proposed RA element was fabricated and its radiation performance was measured. The measured results demonstrated that beam scanning performance of the

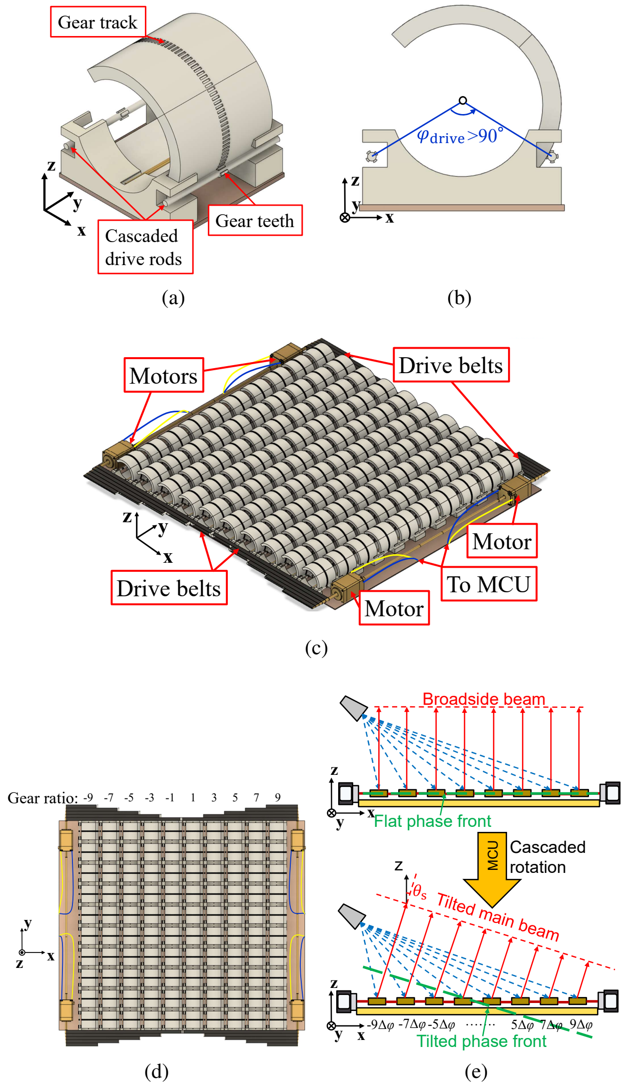

Fig. 11. Conceptual configuration of cylindrical RA for automatically actuation (a). RA element with drive, (b). RA element front view, (c). RA bird eye view, (d). RA front view, (e). working principle.

proposed RA antenna was achieved with acceptable aperture efficiency compared to conventional ones. Also, moderate bandwidth of the proposed RA antenna in comparison with conventional ones was demonstrated.

Future work lies in developing an automatic rotation system for element. For a conceptual example of actuation, 3D-printed dielectric drive rods can be added at 2 lateral sides of the element as shown in Fig. 11(a). Gear track and teeth are printed to drive the force. When the element rotates to state 1, the air-filled section may cause the rods to leave the gear track. The 2 rods are designed at the lateral side of the cylindrical shell and the angle between them φ_{drive} seen from the front view should be larger than 90° open region, which is shown in Fig. 11(b). In this way, there is always at least 1 rod can drive the cylindrical shell to rotate. The rods are cascaded to the adjacent elements on y-axis so that 1 row of cylinder shell on y-axis can be rotated together. To actuate a 10×10 reconfigurable RA shown in Fig. 11(c), 4 motors are used at 4 corners of the RA. A micro control unit (MCU) is placed at the backside of the RA to control the overall rotation of motors. The motors connect to each row of elements by drive belts with different gear ratio in arithmetic sequence which is shown in Fig. 11(d). The gear ratio denotes the rotation speed of specific row when the motors are turned on. The beam scanning principle is shown in Fig. 11(e), that main beam direction can be steered by physical cascaded rotation. For beam scanning to θ_s, the rotation angle $\Delta\varphi$ can be derived by array factor, whereas $2\Delta\varphi = L_x \sin\theta_s/\lambda$. This conceptual belt-driven actuation system can only reconfigure an 1-dimensional beam steering direction.

While the study demonstrated the performance of the proposed RA antenna, several challenging problems still remaining. Expanding the phase-tuning range from the current 270° to a full 360° is a big challenge for enhancing beam scanning performance of the proposed RA antenna. Multi-bit phase tunability is another big challenge for optimizing quantization loss of the proposed RA antenna. Furthermore, miniaturizing the element size is a challenge for applying the proposed RA element for high frequency band. Finally, developing the independent rotation system of single element for reconfiguring the 2-dimensional beam steering. Addressing these challenges can further enhance the performance and capabilities of the proposed RA antenna.

Acknowledgement

The authors would like to acknowledge that the research was financially supported by the World-leading Innovative & Smart Education (WISE) program for Artificial Intelligence and Electronics in Tohoku University and Japan Society for the Promotion of Science (JSPS) KAKENHI Grant Number 22K04061. We would like to appreciate Mr. Narihiro Nakamoto and Dr. Toru Takahashi with Mitsubishi Electric Corporation for their helpful advice on this work

References

[1] D.G. Berry, R.G. Malech, and W.A. Kennedy, "The reflectarray antenna", *IEEE Trans. Antennas Propag.*, vol. 11, no. 6, pp. 645-651, Nov. 1963.

[2] J. Huang, "Analysis of a microstrip reflectarray antenna for microspacecraft applications," *TDA Progress Report 42-120*, pp. 153-173, Feb. 1995.

[3] F. Yang and Y. Rahmat-Samii, Surface Electromagnetics: With Applications in Antenna, Microwave, and Optical Engineering, *Cambridge, U.K.:Cambridge Univ. Press*, Jun. 2019, doi:10.1017/9781108470261.

[4] P. Nayeri, F. Yang and A.Z. Elsherbeni, *Reflectarray Antennas: Theory Designs and Applications*, John Wiley and Sons, 2018. doi:10.1002/9781118846728.

[5] L. Li, Q. Chen, Q. Yuan, K. Sawaya, T. maruyama, T. Furuno, and S. Uebayashi, "Novel Broadband Planar Reflectarray With Parasitic Dipoles for Wireless Communication Applications," *IEEE Antennas Wireless Propag. Lett.*, vol. 8, pp. 881-885, 2009, doi: 10.1109/LAWP.2009.2028298.

[6] P. Callaghan, P. Young and C. Gu, "Corner reflectarray for indoor wireless applications," *in Proc. Antennas and Propagation Conference 2019 (APC-2019)*, pp. 1-5, 2019, doi: 10.1049/cp.2019.0724.

[7] D. Wang, R. Gillard and R. Loison, "A 60GHz passive repeater array with endfire radiation based on metal groove unit-cells," *in Proc. 2015 9th European Conference on Antennas and Propagation (EuCAP)*, pp.1-4, 2015.

[8] S. V. Hum, M. Okoniewski and R. J. Davies, "Realizing an electronically tunable reflectarray using varactor diode-tuned elements," *IEEE Microw. Wireless Comp. Lett.*, vol. 15, no. 6, pp. 422-424, June 2005, doi: 10.1109/LMWC.2005.850561.

[9] E. Carrasco, M. Barba and J. A. Encinar, "X-Band Reflectarray Antenna With Switching-Beam Using PIN Diodes and Gathered Elements," *IEEE Trans. Antennas Propag.*, vol. 60, no. 12, pp. 5700-5708, Dec. 2012, doi: 10.1109/TAP.2012.2208612.

[10] J. Han, L. Li, G. Liu, Z. Wu and Y. Shi, "A Wideband 1 bit 12 × 12 Reconfigurable Beam-Scanning Reflectarray: Design, Fabrication, and Measurement," *IEEE Antennas Wireless Propag. Lett.*, vol. 18, no. 6, pp. 1268-1272, June 2019, doi: 10.1109/LAWP.2019.2914399.

[11] W. Wu, K. D. Xu, Q. Chen, T. Tanaka, M. Kozai and H. Minami, "A Wideband Reflectarray Based on Single-Layer Magneto-Electric Dipole Elements With 1-bit Switching Mode," *IEEE Trans Antennas Propag.*, vol. 70, no. 12, pp. 12346-12351, Dec. 2022, doi: 10.1109/TAP.2022.3209693.

[12] X. Cao, Q. Chen, T. Tanaka, M. Kozai and H. Minami, "A 1-bit Time-Modulated Reflectarray for Reconfigurable-Intelligent-Surface Applications," *IEEE Trans. Antennas Propag.*, vol. 71, no. 3, pp. 2396-2408, March 2023, doi: 10.1109/TAP.2022.3233659.

[13] O. Bayraktar, O. A. Civi and T. Akin, "Beam Switching Reflectarray Monolithically Integrated With RF MEMS Switches," *IEEE Trans. Antennas Propag.*, vol. 60, no. 2, pp. 854-862, Feb. 2012, doi: 10.1109/TAP.2011.2173099.

[14] H. Rajagopalan, Y. Rahmat-Samii and W. A. Imbriale, "RF MEMS Actuated Reconfigurable Reflectarray Patch-Slot Element," *IEEE Trans. Antennas Propag.*, vol. 56, no. 12, pp. 3689-3699, Dec. 2008, doi: 10.1109/TAP.2008.2007388.

[15] W. Zhang, Y. Li and Z. Zhang, "A Reconfigurable Reflectarray Antenna With an 8 μm-Thick Layer of Liquid Crystal," *IEEE Trans. Antennas Propag.*, vol. 70, no. 4, pp. 2770-2778, April 2022, doi: 10.1109/TAP.2021.3125378.

[16] X. Li, H. Sato, Y. Shibata, T. Ishinabe, H. Fujikake and Q. Chen, "Development of Beam Steerable Reflectarray With Liquid Crystal for Both E-Plane and H-Plane," *IEEE Access*, vol. 10, pp. 26177-26185, 2022, doi: 10.1109/ACCESS.2022.3155544.

[17] R. L. Haupt and M. Lanagan, "Reconfigurable Antennas," *IEEE Antennas Propag. Mag.*, vol. 55, no. 1, pp. 49-61, Feb. 2013, doi: 10.1109/MAP.2013.6474484.

[18] L. Liu, F. Yang, S. Xu and M. Li, "A 2-Bit Reconfigurable Reflectarray Unit Design Using Only 2 PIN Diodes," *in Proc. 2022 IEEE MTT-S International Microwave Workshop Series on Advanced Materials and Processes for RF and THz Applications (IMWS-AMP)*, pp. 1-2, 2022, doi: 10.1109/IMWS-AMP54652.2022.10107038.

[19] F. Wu, W. Zhao, X. Xia, J. Wang, Z. H. Jiang, R. Sauleau and W. Hong, "A 2 bit Circularly Polarized Reconfigurable Reflectarray Using p-i-n-Diode-Tuned Crossed-Bowtie Patch Elements," *IEEE Trans. Antennas Propag.*, vol. 71, no. 9, pp. 7299-7309, Sept. 2023, doi: 10.1109/TAP.2023.3291773.

[20] X. Yang, S. Xu, F. Yang, M. Li, H. Fang, Y. Hou, S. Jiang and L. Liu, "A Mechanically Reconfigurable Reflectarray With Slotted Patches of Tunable Height," *IEEE Antennas Wireless Propag. Lett.*, vol. 17, no. 4, pp. 555-558, April 2018, doi: 10.1109/LAWP.2018.2802701.

[21] J. P. Gianvittorio and Y. Rahmat-Samii, "Reconfigurable patch antennas for steerable reflectarray applications," *IEEE Trans. Antennas Propag.*, vol. 54, no. 5, pp. 1388-1392, May 2006, doi: 10.1109/TAP.2006.874311.

[22] A. Hu, K. Konno, Q. Chen and T. Takahashi, "A Highly Efficient 1-bit Reflectarray Antenna Using Electromagnets-Controlled Elements," *IEEE Trans. Antennas Propag.*, vol. 72, no. 1, pp. 506-517, doi: 10.1109/TAP.2023.3324457.

[23] V. F. Fusco, "Mechanical beam scanning reflectarray," *IEEE Trans. Antennas Propag.*, vol. 53, no. 11, pp. 3842-3844, Nov. 2005, doi: 10.1109/TAP.2005.858828.

[24] X. Yang, S. Xu, F. Yang, M. Li, Y. Hou, S. Jiang, and L. Liu, "Broadband high-efficiency reconfigurable reflectarray antenna using mechanically rotational elements," *IEEE Trans. Antennas Propag.*, vol. 65, no. 8, pp. 3959-3966, Aug. 2017.

[25] Y. Cui, S. A. Nauroze, R. Bahr and E. M. Tentzeris, "3D Printed One-shot Deployable Flexible "Kirigami" Dielectric Reflectarray Antenna for mm-Wave Applications," *in Proc. 2020 IEEE/MTT-S International Microwave Symposium (IMS)*, pp. 1164-1167, 2020, doi: 10.1109/IMS30576.2020.9224010.

[26] C. Benteyn, R. Gillard, E. Fourn, G. Goussetis, H. Legay and L. Datashvili, "A Design Methodology for Reconfigurable Reflectarrays with a Deformable Ground," *in Proc. 2020 14th European Conference on Antennas and Propagation (EuCAP)*, pp. 1-5, 2020, doi: 10.23919/EuCAP48036.2020.9135257.

[27] M. I. Abbasi, M. H. Dahri, M. H. Jamaluddin, N. Seman, M. R. Kamarudin and N. H. Sulaiman, "Millimeter Wave Beam Steering Reflectarray Antenna Based on Mechanical Rotation of Array," *IEEE Access*, vol. 7, pp. 145685-145691, 2019, doi: 10.1109/ACCESS.2019.2945318.

[28] Z. Cao, Y. Li, Z. Zhang and M. F. Iskander, "Single Motor-Controlled Mechanically Reconfigurable Reflectarray," *IEEE Trans. Antennas Propag.*, vol. 71, no. 1, pp. 190-199, Jan. 2023, doi: 10.1109/TAP.2022.3221036.

[29] P. Nayeri, M. Liang, R. A. S. Garcia, M. Tuo, F. Yang, M. Gehm, H. Xin and A. Z. Elsherbeni, "3D Printed Dielectric Reflectarrays: Low-Cost High-Gain Antennas at Sub-Millimeter Waves," *IEEE Trans. Antennas Propag.*, vol. 62, no. 4, pp. 2000-2008, April 2014, doi: 10.1109/TAP.2014.2303195.

[30] J. Zhu, Y. Yang, D. Mcgloin, S. Liao and Q. Xue, "3-D Printed All-Dielectric Dual-Band Broadband Reflectarray With a Large Frequency Ratio," *IEEE Trans. Antennas Propag.*, vol. 69, no. 10, pp. 7035-7040, Oct. 2021, doi: 10.1109/TAP.2021.3076528.

[31] V. Basile, V. Marrocco, M. Spina, I. Fassi, A. D'orazio and M. Grande, "3D Printed Micro-Cells for Phase Control in 5G mmWave Applications," *IEEE Access*, vol. 9, pp. 46049-46060, 2021, doi: 10.1109/ACCESS.2021.3068130.

[32] W. Wu, K. D. Xu, Q. Chen, T. Tanaka, M. Kozai and H. Minami, "A Low-Cost Wideband Reflectarray Antenna Based on Nonradiative Dielectric Waveguide," *IEEE Antennas Wireless Propag. Lett.*, early access

[33] K. Yokokawa, K. Konno and Q. Chen, "Scattering Performance of Log-Periodic Dipole Array," *IEEE Antennas Wireless Propag. Lett.*, vol. 16, pp. 740-743, 2017, doi: 10.1109/LAWP.2016.2601244.

[34] H. Ito, K. Konno, H. Sato and Q. Chen, "Wideband Scattering Performance of Reflectarray Using Log-Periodic Dipole Array," *IEEE Antennas Wireless Propag. Lett.*, vol. 16, pp. 1305-1308, 2017, doi: 10.1109/LAWP.2016.2633305.

[35] S. V. Hum and J. Perruisseau-Carrier, "Reconfigurable Reflectarrays and Array Lenses for Dynamic Antenna Beam Control: A Review," *IEEE Trans. Antennas Propag.*, vol. 62, no. 1, pp. 183-198, Jan. 2014, doi: 10.1109/TAP.2013.2287296.

[36] S. Zhang, Y. Vardaxoglou, W. Whittow and R. Mittra, "3D-printed graded index lens for RF applications," *in Proc. 2016 International Symposium on Antennas and Propagation (ISAP)*, pp. 90-91, 2016.

[37] M. I. Hossain, N. Nguyen-Trong and A. M. Abbosh, "Calibrated Parallel-Plate Waveguide Technique for Low-Frequency and Broadband Absorptivity Measurement," *IEEE Antennas Wireless Propag. Lett.*, vol. 19, no. 9, pp. 1541-1545, Sept. 2020, doi: 10.1109/LAWP.2020.3008889.

[38] Y. Shang, Z. Shen and S. Xiao, "On the Design of Single-Layer Circuit Analog Absorber Using Double-Square-Loop Array," *IEEE Trans. Antennas Propag.*, vol. 61, no. 12, pp. 6022-6029, Dec. 2013, doi: 10.1109/TAP.2013.2280836.

[39] L. Zhou and Z. Shen, "3-D Absorptive Energy-Selective Structures," *IEEE Trans. Antennas Propag.*, vol. 69, no. 9, pp. 5664-5672, Sept. 2021, doi: 10.1109/TAP.2021.3061097.

[40] A-Info Technical Specification, LB-187-10 Data sheet, http://www.ainfoinc.com.cn/en/pro_pdf/new_products/antenna/Standard%20Gain%20Horn%20Antenna/tr_LB-187-10.pdf (Accessed 2023-11-15)

[41] H. Yang, F. Yang, S. Xu, Y. Mao, M. Li, X. Cao, and J. Gao, , "A 1-Bit 10×10 Reconfigurable Reflectarray Antenna: Design, Optimization, and Experiment," *IEEE Trans. Antennas Propag.*, vol. 64, no. 6, pp. 2246-2254, June 2016, doi: 10.1109/TAP.2016.2550178.

[42] J. Huang and R. J. Pogorzelski, "A Ka-band microstrip reflectarray with elements having variable rotation angles," *IEEE Trans. Antennas Propag.*, vol. 46, no. 5, pp. 650-656, May 1998, doi: 10.1109/8.668907.

[43] D. M. Pozar, S. D. Targonski and H. D. Syrigos, "Design of millimeter wave microstrip reflectarrays," *IEEE Trans. Antennas Propag.*, vol. 45, no. 2, pp. 287-296, Feb. 1997, doi: 10.1109/8.560348.

Ao Hu received B.E degree from Huazhong University of Science and Technology, Wuhan, China, in 2018, and M.Sc degree from KTH Royal Institute of Technology, Stockholm, Sweden, in 2019. He is currently pursuing Ph.D degree at Tohoku University, Sendai, Japan. He is also a student member with AIE-WISE Program for AI Electronics of Tohoku University. His research interests include mechanically-actuated reflectarray antennas and reconfigurable intelligent surface.

Keisuke Konno (M'12) received the B.E., M.E., and D.E. degrees from Tohoku University, Sendai, Japan, in 2007, 2009, and 2012, respectively. Since 2012, he has been with the Department of Communications Engineering, Graduate School of Engineering, Tohoku University, where he is an Associate Professor. He received a JSPS Postdoctral Fellowships for Research Abroad and he was staying with the ElectroScience Laboratory, the Ohio State University, as a visiting scholar from 2015 to 2017. His research interests include computational electromagnetics, array antennas, reflectarrays, and source reconstruction. Dr. Konno is a member of IEEE and IEICE.

He received the Encouragement Award for Young Researcher and Most Frequent Presentations Award in 2010 from the Technical Committee on Antennas and Propagation of Japan, Young Researchers Award in 2011 from the Institute of Electronics, Information and Communication Engineers (IEICE) of Japan, IEEE EMC Society Sendai Chapter Student Brush-up Session & EMC Sendai Seminar Student Best Presentation Award in 2011, JSPS Washington Director Award in 2016, MHz Rectenna Award in 2017, Young Researchers Award for ECEI of Tohoku University in 2018, Minoru Ishida Award in 2018, IEEE AP-S Japan Young Engineer Award in 2018, TOKIN Foundation Research Encouragement Award in 2019, IEICE Communications Society Distinguished Contributions Award in 2019.

Qiang Chen received the B.E. degree from Xidian University, Xi'an, China, in 1986, the M.E. and D.E. degrees from Tohoku University, Sendai, Japan, in 1991 and 1994, respectively. He is currently an Associate Professor with the Department of Communications Engineering, Tohoku University. His primary research interests include computational electromagnetics, array antennas, and antenna measurement.

Dr. Chen received the Young Scientists Award in 1993, the Best Paper Award and Zen-ichi Kiyasu Award in 2009 from the Institute of Electronics, Information and Communication Engineers (IEICE) of Japan. Dr. Chen is a member of the IEEE and IEICE. He was the Secretary and Treasurer of IEEE Antennas and Propagation Society Japan Chapter in 1998, the Secretary of Technical Committee on Electromagnetic Compatibility of IEICE from 2004 to 2006, the Secretary of Technical Committee on Antennas and Propagation of IEICE from 2008 to 2010, Associate Editor of IEICE Transactions on Communications from 2007 to 2012. He is Chair of IEICE Technical Committee on Photonics-applied Electromagnetic Measurement.